Fiber-based Frequency Modulated LiDAR With MEMS Scanning Capability for Long-range Sensing in Automotive Applications

Conference Paper · July 2021

CITATIONS
0

READS
74

18 authors, including:

Sarah Cwalina
Fraunhofer-Institut für Nachrichtentechnik, Heinrich-Hertz-Institut
2 PUBLICATIONS **0** CITATIONS
SEE PROFILE

Christoph Kottke
Fraunhofer-Gesellschaft zur Förderung der angewandten Forschung e.V.
61 PUBLICATIONS **1,645** CITATIONS
SEE PROFILE

Volker Jungnickel
Fraunhofer-Institut für Nachrichtentechnik, Heinrich-Hertz-Institut
278 PUBLICATIONS **6,124** CITATIONS
SEE PROFILE

Pascal Rustige
Fraunhofer-Institut für Nachrichtentechnik, Heinrich-Hertz-Institut
12 PUBLICATIONS **8** CITATIONS
SEE PROFILE

Fiber-based Frequency Modulated LiDAR With MEMS Scanning Capability for Long-range Sensing in Automotive Applications

Sarah Cwalina[1], Christoph Kottke[1], Volker Jungnickel[1], Ronald Freund[1], Patrick Runge[1], Pascal Rustige[1], Thomas Knieling[2], Shanshan Gu-Stoppel[2], Jörg Albers[2], Norman Laske[2], Frank Senger[2], Lianzhi Wen[2], Fabio Giovanneschi[3], Erdem Altuntac[3], Avinash Nittur Ramesh[3], María A. González-Huici[3], Andries Küter[3], and Sangeeta Reddy[3]

[1]Fraunhofer HHI, Berlin, Germany, email: sarah.cwalina@hhi.fraunhofer.de
[2]Fraunhofer ISIT, Itzehoe, Germany
[3]Fraunhofer FHR, Wachtberg, Germany

***Abstract*—Safe operation of driver assistance systems, especially at higher speeds, remains a challenge. For this automotive application, we propose a long-range coherent LiDAR system concept with two-dimensional micro electro-mechanical system (MEMS) scanning and sparse sensing capability. We address system design challenges for the transmitter, the fiber-based optics and coherent receiver, and the impact on MEMS mirror design. Furthermore, we compare compressed sensing and deep learning techniques to implement sparse sensing and we provide preliminary results of the systems performance with a simplified setup.**

***Index Terms*—advanced driver assistance systems (ADAS), coherent systems, compressed sensing, deep learning, frequency modulated continuous wave (FMCW), LiDAR, MEMS mirror, sensing**

I. Introduction

LiDAR (Light Detection and Ranging) is seen by the automotive industry as a critical and important step in the advancement of driver assistance systems (ADAS). The automotive application requires LiDAR to be eye-safe, reach a long range, generate a dense point cloud and ideally fit in a small form-factor. Especially coherent LiDAR concepts have gained attraction in recent years [1] [2], because they promise to reach long distances and have a built-in mitigation of interference (e.g. from bright sunlight). Both of which are increasing the safe operation of ADAS at higher speeds and different weather conditions.

Optical frequency comb (OFC) [3] [4] and frequency modulated continuous wave (FMCW) [5] [6] are the two main coherent principles that have prevailed. OFC is based on a phase locked optical comb with uniform spacing in the frequency domain that undergoes a phase shift during propagation. FMCW, known from RADAR technology and chosen for the system presented here, is based on a frequency modulated optical carrier.

Previous demonstrations of FMCW ranging show various system designs. For example, the generation of the frequency modulation is either realized by external modulation (e.g. using carrier suppressed IQ modulators) [7] or direct modulation of a laser [8]. Fiber-based FMCW LiDARs aimed at wind sensing or range finding applications have been demonstrated [9] [5] with several kilometer range. However, they lack the capability to scan a field of view (FOV), which is necessary for automotive applications, and proves to be challenging in combination with coherent techniques. A common approach is the use of image sensors [10] or mechanical beam steering systems [11], which can be bulky and slow. Other concepts include the supplementary use of a dispersive element [12] or grating couplers [8] for one dimension of scanning.

To our best knowledge, we show the first system design of a (fiber-based) directly modulated FMCW LiDAR with two-dimensional MEMS mirror scanning capability. The combination offers a low-cost, miniaturized approach that addresses the price-driven automotive market. Additionally, we propose to perform sparse sensing in combination with advanced signal processing methods based on Compressed Sensing or Deep Learning techniques for full scene recovery. This will allow a higher efficiency of hardware usage along with a faster scan rate, which is crucial in dynamic scenarios. Simultaneous velocity information is also available with the coherent approach, but this is beyond the scope of this paper.

The remainder of this paper is organized as follows. The FMCW coherent LiDAR method is introduced in section II. In section III, the proposed system is presented structured according to its building blocks. Lastly, measurement examples of a preliminary prototype are shown in section IV.

II. FMCW method

For any LiDAR, the distance to an object is obtained by light reflecting at an object and returning to the receiver. FMCW LiDAR differs particularly in how the distance information is retrieved. Whereas a time-of-flight (ToF) system directly measures the time it takes for light to travel to the object, an FMCW system measures this time indirectly from optical mixing of the returning signal with a reference. Fig. 1

This work was supported by Fraunhofer-Gesellschaft

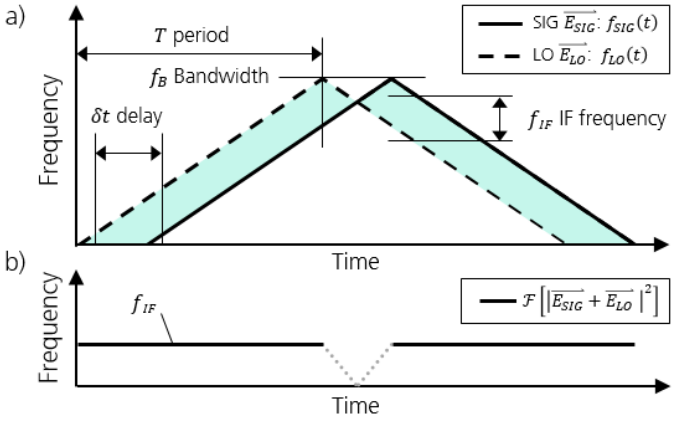

Fig. 1. FMCW principle for static object ranging. a) The signal (SIG) consists of a rising and falling linear frequency modulation (bandwidth f_B, period T). Compared to the local oscillator (LO) which inhibits the same frequency modulation, the SIG is delayed by δt due to the additional path of the object reflection. b) The spectrogram of heterodyne mixing of SIG and LO shows the IF frequency f_{IF} due to the delay.

shows the principle of FMCW. A continuous wave laser is linearly frequency modulated, i.e. chirped, by the modulation bandwidth f_B within a period T (by the rate $R = f_B/T$). Due to the delay δt between the retrieved signal (SIG) and the local oscillator (LO) the heterodyne mixing produces an intermediate frequency f_{IF}, which translates back to the distance d of the object:

$$d = f_{IF}\frac{cn}{2R}, \tag{1}$$

where c is the speed of light and n is the refractive index of the medium. The IF frequency can be obtained by spectral analysis of the mixed signal $\|\vec{E_{SIG}} + \vec{E_{LO}}\|^2$ at the coherent receiver using the fast Fourier transform (FFT).

Using this coherent LiDAR method allows a larger detection range (limited by the coherence length of the laser) and an inherent interference signal filter. The following section discusses how this method is embedded in the system and its impact on system design.

III. System Design and Results

Fig. 2 shows the building blocks of the LiDAR system. The system operates at $1550\,\mathrm{nm}$ which allows higher eye-safe power and less sunlight noise compared to wavelengths around $900\,\mathrm{nm}$ [13]. It also allows us to use standard telecom components for the transmitter and receiver, as well as fiber-based optics for the sensor head. Scanning is realized by a micro-engineered 2D MEMS mirror providing directional illumination. Furthermore, sparse sensing techniques enable fast scanning and reconstruction of the scene.

A. Transmitter

For the transmitter, a tunable ultra-narrow linewidth ($100\,\mathrm{kHz}$) laser diode is used. The lasers bias current is modulated directly using an arbitrary waveform generator as a driver. The modulation of the injected current results in a frequency modulation due to the change of refractive index in the cavity [14] and temperature. In theory, the cavity effect

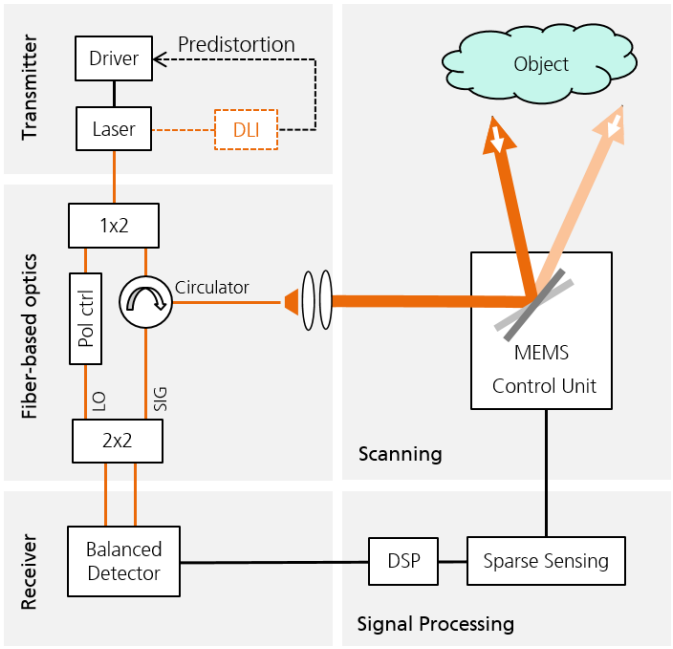

Fig. 2. LiDAR system consisting of transmitter, fiber-based optics, receiver, signal processing and scanning unit. Optical fiber shown in orange, electrical connections shown in black.

shows a refractive index variation proportional to the carrier density. Therefore, the linear frequency modulation should be proportional to the linear bias modulation (dynamic spectral shift). For our laser, a current tuning coefficient of around $3\,\mathrm{pm/mA}$ is given. However, dynamic non-linearity and the additional temperature tuning effect results in a non-linear behavior that requires a predistortion of the modulation.

Predistortion: A quadratic predistortion of the bias modulation is assumed. Hereby, the rising and falling chirp is affected by different non-linear dynamics and therefore handled separately. Equation 2 shows the quadratic predistortion $p(t)$ for the rising and falling frequency modulation with the respective non-linearity factors a, b and the sample size S of one period.

$$\begin{aligned} p_{rise}(t) &= -t^2 + aSt, \quad t = [-S, 0] \\ p_{fall}(t) &= +t^2 - bSt, \quad t = [0, S] \end{aligned} \tag{2}$$

The influence of the predistortion is illustrated in Fig. 3: A measurement of the FMCW spectrogram in a $14\,\mathrm{ns}$ delay line interferometer (DLI) with triangular bias modulation. Fig. 1 b) shows the ideal plot of the spectrogram and thus serves as a comparison for Fig. 3. The IF frequency is expected to be constant around $1\,\mathrm{MHz}$ in this configuration. The non-predistorted measurement is shown in Fig. 3 a). A temporal variation of the IF frequency from around $0.5\,\mathrm{MHz}$ to $1.1\,\mathrm{MHz}$ is visible. The predistorted ($a = 2.2$, $b = 7.2$) measurement is shown in Fig. 3 b) and shows less variation of the IF frequency (from around $0.7\,\mathrm{MHz}$ to $1\,\mathrm{MHz}$). One can see that the predistortion decreases the temporal variation of the IF frequency in the spectrogram. This results in a smaller linewidth of the FFT power spectrum, when performed over the entire time domain.

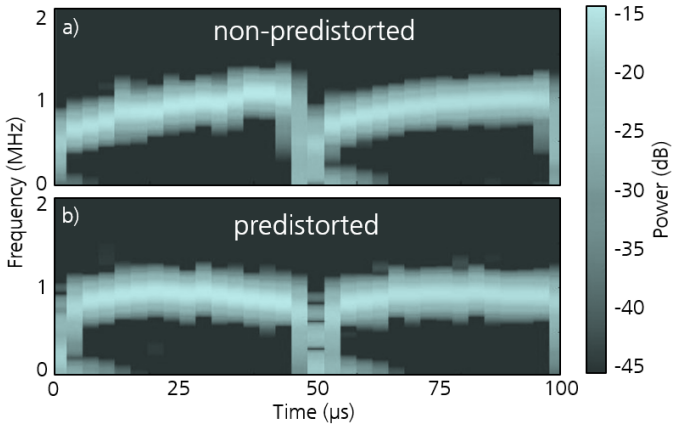

Fig. 3. Spectrogram of FMCW ($T = 50\,\mu s$, $f_B = 3.6\,GHz$) mix signal in a fiber-based 14 ns DLI: a) No predistortion of the laser bias modulation. b) With predistortion. The frequency resolution is 200 kHz and the time resolution 12.83 µs. Refer to Fig. 1 b) for the spectrogram's ideal shape.

B. Fiber-based Optics

The characteristic of coherent detection is the optical heterodyne mixing of a signal with its reference. In our system, all optical connections are realized by single mode fiber components. The transmitters output is split into a SIG and reference (LO) branch and combined again with matching polarizations for the optical mixing. In-between, the signal is guided through an optical circulator onto the scanning unit by a fiber-coupled collimator. The object is illuminated and its reflection is received on the same path.

The optical design challenge lies in the combination of a fiber coupled collimator, the eye-safety limitations and the MEMS mirror aperture for receiving (and transmitting) enough optical power. In short, when using optical fibers on the receiving end, a collimator is required as the lens. The aperture of the collimator (and correspondingly the aperture of the MEMS mirror) becomes a limiting factor of the received power [15].

C. Receiver

In a first approach, we develop an InP coherent receiver for 1550 nm optical wavelength based on waveguide-integrated balanced photodetectors [16] in a 180° hybrid 2x2 MMI configuration, matching the fiber-coupled configuration of typical coherent LiDAR setups. To overcome the afore-mentioned optical design challenge of efficiently coupling the received signal from various solid angles into the single mode fiber (see Sec. III-D), we also investigate a free-space coherent receiver approach [17].

D. Scanning

MEMS mirror development for a certain application is always like finding a sweet spot between its physical parameters mirror mass (depending on thickness, diameter), FOV (which is four times of its mechanical scan angle) and its oscillation frequency which directly determines its response and decay times. In addition, quasi-static mirrors for this LiDAR application require a robust actuator design and a powerful drive principle.

We are developing a quasi-static MEMS mirror with a novel design and powerful piezoelectric driving material of AlN/AlScN where the latter offers at least four times higher piezoelectric efficiency than AlN. Material properties like mechanical stress and piezoelectric efficiency will be further optimized. It has large mechanical tilt angles and high frequencies as well as great long-term stability and linearity [18]. An initial set of mirrors has been manufactured, mounted on a PCB and tested. (see Fig. 4).

A novel three wafer bonding process based on glass fritting has been developed for maximizing fill-factor and enhancing mechanical linearity. Here, the mirror plate and actuators are on different heights and vertical electrical contacts are implemented. [19]. Optical hermetic sealing improves the mechanical robustness of the quasi-static MEMS components and protects them from the particles and humidity from the environment. With this new process, quasi-static mirrors with diameters ranging from 2 mm to 10 mm with high linearity, high mechanical robustness and large tilting angles have been fabricated [20]. Table I shows the competing parameters for a selection of three mirror designs.

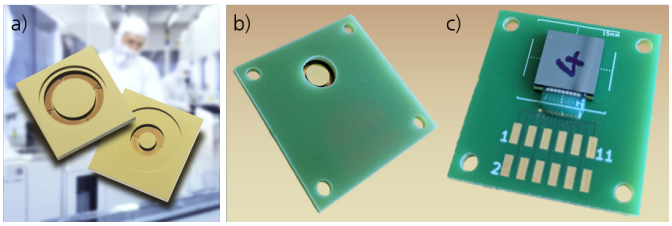

Fig. 4. Gold coated MEMS mirror chips a) Design for 2 mm and 5 mm. These mirrors (5 mm aperture) are manufactured, assembled and tested: b) Front view. c) Back view.

TABLE I
MIRROR DESIGNS AND PARAMETERS.

Aperture	2 mm	5 mm	10 mm
Field of view	> 20° x 20°	20° x 20°	15° x 15°
Min. response time	154 µs	286 µs	5 ms
Highest working frequency	6.5 kHz	3.5 kHz	200 Hz

E. Signal Processing

The scanning unit needs to aim at a single identical spot for the complete duration of the measurement cycle. The time it takes to drive the MEMS mirror into position (defined by its working frequency) and subsequently perform the measurement defines a lower bound for the scan rate of the LiDAR. It is therefore desirable to operate the system within tight timing margins. Hence, we are using a field-programmable gate array (FPGA) as they are ideally suited to provide cycle accurate system-wide trigger signals and synchronize the necessary acquisition steps [21]. So far, the FPGA is included in a System-on-Chip (SoC) that also integrates microprocessor

cores to run an embedded Linux operating system. This in turn enables faster prototyping of signal processing steps that we will synthesize into hardware later on.

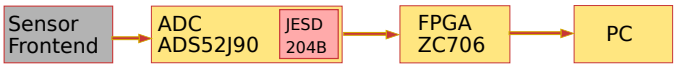

Fig. 5. Data flow diagram (simplified)

The FPGA portion of the SoC also handles the measurement data acquisition (see Fig. 5). Currently, we acquire the raw data using an ADC with $65\,\mathrm{MS/s}$ and $14\,\mathrm{bit}$ resolution. We offload the filtered data into a host PC using a PCI-Express interface and store it for offline processing. Using general-purpose IP cores, we achieve a sustained data rate $>180\,\mathrm{MB/s}$ for our setup, which is sufficient for the current state of the system that outputs $130\,\mathrm{MB/s}$ in continuous operation.

F. Sparse Sensing

One of the innovative features of this system is an improved scanning rate enabled by sparse sensing and realized by either random (or even adaptive) MEMS mirror pattern tracing. To this end, we analyze compressed sensing and deep learning techniques to generate dense point clouds from incomplete or sparse LiDAR measurements using the KITTI dataset [22] as benchmark.

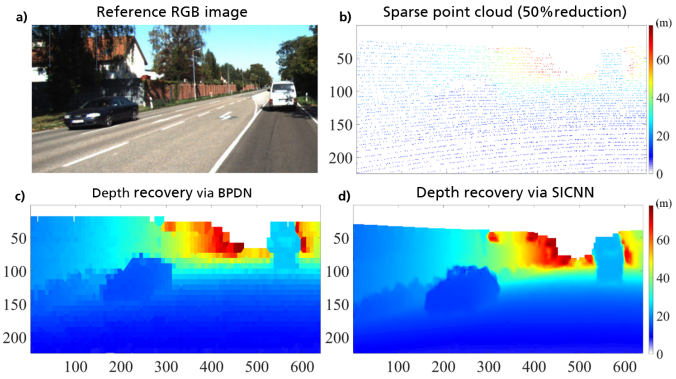

Fig. 6. a) Reference RGB image of the selected KITTI snapshot, b) the considered point cloud after 50% data reduction, and the dense depth maps obtained c) via CS (BPDN) and d) Deep Learning (SICNN).

Compressed sensing is a well-established mathematical theory that provides conditions and efficient methods for the reconstruction of signals that are compressible from only a few (e.g. random) samples [23]. CS has been proposed for LiDAR acquisition and processing only in recent years, with special emphasis on reducing scanning time [24]. We employ CS algorithms based on the Basis Pursuit Denoising (BPDN) problem [25] [26] using Wavelets and DFT domains.

Deep learning techniques applied to LiDAR [27] [28] rely on multi-modal sensor data, and use datasets of ground truth depth images for training and inference. We implemented a Sparsity Invariant Convolutional Neural Network (SICNN) [29] where Synthia dense dataset [30] is used for training the network and KITTI data is used to fine-tune the training phase through transfer learning.

Figure 6 shows an examplary result of depth recovery with BPDN and SICNN from a snapshot of the KITTI dataset where we randomly annihilated 50% of the data from the original and already sparse point cloud. Both techniques generate dense depth images where the illuminated scene is recovered with a very low Mean Absolute Error on the depth values ($71.8\,\mathrm{cm}$ for BPDN and $38.5\,\mathrm{cm}$ for SICNN). So far, we have observed a satisfactory performance up to a 20% annihilation of data. Next steps will include the development of a constrained CS algorithm for an improved recovery of object shapes and the development of synthetic ground truths to simulate several scenarios to be used for SICNN training.

IV. Measurement Results

First measurements were performed in an outdoor setting with a simplified setup (without scanning, and sparse sensing, with commercial balanced photodetector and simple offline signal processing) to verify the working principle and assess the systems limitations. The optical sensor head was aimed at a paper target at specific distances. All transmitter parameters were set according to the previous description ($T = 50\,\mu\mathrm{s}$, $f_B = 3.6\,\mathrm{GHz}$, $a = 2.2$, $b = 7.2$).

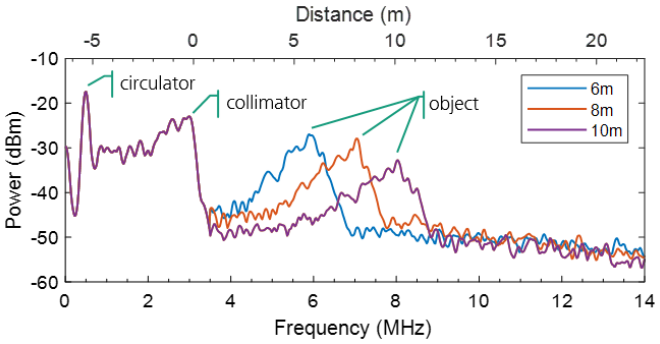

Fig. 7. FMCW power spectrum for selected target distances (6 m-10 m). The reflection at the circulator, collimator and the target object produce different IF frequencies. Distance scale calculated according to Eq. 1 and shifted by the calibration.

A selection of measurements are shown in Fig. 7. The trace of the curve shows peaks for every reflection along the light path because the returned signal at each reflection produces a different IF frequency. As a result, we can calibrate the distance calculation to the last reflective surface; the collimator lens. Using a peak finding algorithm, distances of object reflections are calculated. The broad target reflection peak indicates a need for systematic optimization of the predistortion, which is currently investigated.

A comparison of the intended target distances and the distances calculated from the IF frequency is shown in Fig. 8. They are in good accordance, the total discrepancy is below $1\,\mathrm{m}$ for each of the measurements. Additionally, Fig. 8 shows the signal to noise ratio (SNR), which is above $10\,\mathrm{dB}$ for all measurements up to $30\,\mathrm{m}$.

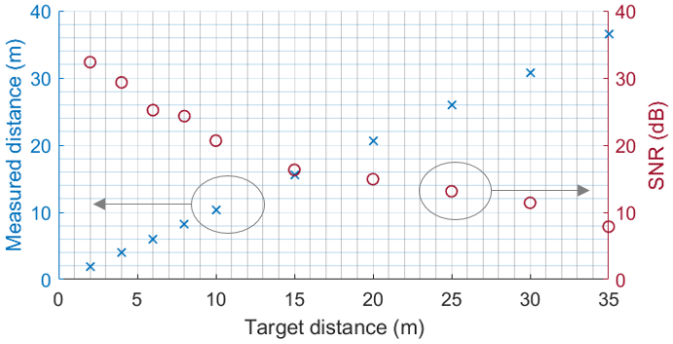

Fig. 8. Calculated distances and signal to noise ratio (SNR) relating to the IF frequency peak in the FMCW power spectrums. The intended target distances are in the range of 2 m-35 m.

V. Conclusion

We present a novel long-range LiDAR system concept targeting the automotive market. Our design combines frequency modulated continuous wave (FMCW) coherent detection with two-dimensional scanning capability and sparse sensing. We discuss the design challenges of each subsystem and their impact on the system performance. The transmitter requires predistortion to reduce the width of the object's reflection peak. Fiber-based optics allow the use of standard telecom receiver components but leads to challenges in optical coupling. A larger aperture of the micro electro-mechanical system (MEMS) mirror could mitigate optical coupling challenges but leads to a slower drive frequency and thus a reduced scan rate. However, the implementation of sparse sensing and advanced signal processing techniques allow a complete reconstruction of the scene with a smaller number of points, increasing the scan rate in turn. Therefore, we show exemplary results of sparse sensing by comparing deep learning and compressed sensing techniques.

References

[1] P. Boulay and A. Debray, "Lidar for automotive and industrial applications - challenges and market opportunities," YOLE Développement, 2019.

[2] J. Hecht, "Lasers for lidar: Fmcw lidar: An alternative for self-driving cars," May 2019. [Online]. Available: https://www.laserfocusworld.com/home/article/16556322/lasers-for-lidar-fmcw-lidar-an-alternative-for-selfdriving-cars

[3] C. Weimann, F. Hoeller, Y. Schleitzer, C. A. Diez, B. Spruck, W. Freude, Y. Boeck, and C. Koos, "Measurement of length and position with frequency combs," *Journal of Physics: Conference Series*, vol. 605, p. 012030, 2015.

[4] P. Trocha, M. Karpov, D. Ganin, M. H. P. Pfeiffer, A. Kordts, S. Wolf, J. Krockenberger, P. Marin-Palomo, C. Weimann, S. Randel, and et al., "Ultrafast optical ranging using microresonator soliton frequency combs," *Science*, vol. 359, no. 6378, p. 887–891, 2018.

[5] F. Amzajerdia and D. Pierrottet, "Fiber-based coherent lidar for target ranging, velocimetry, and atmospheric wind sensing," 2006.

[6] B. Behroozpour, P. A. M. Sandborn, N. Quack, T.-J. Seok, Y. Matsui, M. C. Wu, and B. E. Boser, "Electronic-photonic integrated circuit for 3d microimaging," *IEEE Journal of Solid-State Circuits*, vol. 52, no. 1, 2017.

[7] S. Gao and R. Hui, "Frequency-modulated continuous-wave lidar using iq modulator for simplified heterodyne detection," *optics letters*, vol. 37, no. 11, 2012.

[8] A. Martin, P. Verheyen, P. D. Heyn, P. Absil, P. Feneyrou, J. Bourderionnet, D. Dodane, L. Leviandier, D. Dolfi, A. Naughton, and et al., "Photonic integrated circuit-based fmcw coherent lidar," *Journal of Lightwave Technology*, vol. 36, no. 19, p. 4640–4645, 2018.

[9] P. Feneyrou, L. Leviandier, J. Minet, G. Pillet, A. Martin, D. Dolfi, J.-P. Schlotterbeck, P. Rondeau, X. Lacondemine, A. Rieu, and et al., "Frequency-modulated multifunction lidar for anemometry, range finding, and velocimetry—2 experimental results," *Applied Optics*, vol. 56, no. 35, p. 9676, 2017.

[10] L. Frey, A. Daami, F. Rigal, and D. Muhire, "Three dimensional fmcw scanless imaging: optical challenges and solutions," *Photonic Instrumentation Engineering VIII*, 2021.

[11] R. K. Ula, Y. Noguchi, and K. Iiyama, "Three-dimensional object profiling using highly accurate fmcw optical ranging system," *Journal of Lightwave Technology*, vol. 37, no. 15, p. 3826–3833, 2019.

[12] M. Okano and C. Chong, "Swept source lidar: simultaneous fmcw ranging and nonmechanical beam steering with a wideband swept source," *Optics Express*, vol. 28, no. 16, p. 23898, 2020.

[13] IEC 60825, "Safety of laser products - part 1: Equipment classification and requirements," International Electrotechnical Commission, Standard, 2014.

[14] L. A. Coldren, S. W. Corzine, and M. L. Masanovic, *Diode lasers and photonic integrated circuit*. Wiley, 2012, pp. 452 – 473.

[15] D. Wang, C. Watkins, and H. Xie, "Mems mirrors for lidar: A review," *Micromachines*, vol. 11, no. 5, p. 456, 2020.

[16] P. Runge, G. Zhou, T. Beckerwerth, F. Ganzer, S. Keyvaninia, S. Seifert, W. Ebert, S. Mutschall, A. Seeger, M. Schell, and et al., "Waveguide integrated balanced photodetectors for coherent receivers," *IEEE Journal of Selected Topics in Quantum Electronics*, vol. 24, no. 2, p. 1–7, 2018.

[17] P. Rustige, P. Runge, F. M. Soares, J. Krause, and M. Schell, "A new concept for spatially resolved coherent detection with vertically illuminated photodetectors targeting ranging applications," in *Optical Components and Materials XVIII*, S. Jiang and M. J. F. Digonnet, Eds., vol. 11682, International Society for Optics and Photonics. SPIE, 2021, pp. 18 – 24. [Online]. Available: https://doi.org/10.1117/12.2576323

[18] S. Gu-Stoppel, T. Lisec, M. Claus, N. Funck, S. Fichtner, S. Schröder, B. Wagner, and F. Lofink, "A triple-wafer-bonded AlScN driven quasi-static MEMS mirror with high linearity and large tilt angles," in *MOEMS and Miniaturized Systems XIX*, W. Piyawattanametha, Y.-H. Park, and H. Zappe, Eds., vol. 11293, International Society for Optics and Photonics. SPIE, 2020, pp. 20 – 26. [Online]. Available: https://doi.org/10.1117/12.2542800

[19] S. Gu-Stoppel, F. Senger, L. Wen, E. Yarar, G. Wille, and J. Albers, "A designing and manufacturing platform for AlScN based highly linear quasi-static MEMS mirrors with large optical apertures," in *MOEMS and Miniaturized Systems XX*, H. Zappe, W. Piyawattanametha, and Y.-H. Park, Eds., vol. 11697, International Society for Optics and Photonics. SPIE, 2021, pp. 106 – 115. [Online]. Available: https://doi.org/10.1117/12.2583399

[20] S. Gu-Stoppel, T. Lisec, S. Fichtner, N. Funck, C. Eisermann, F. Lofink, B. Wagner, and A. Müller-Groeling, "A highly linear piezoelectric quasi-static MEMS mirror with mechanical tilt angles of larger than 10° ," in *MOEMS and Miniaturized Systems XVIII*, W. Piyawattanametha, Y.-H. Park, and H. Zappe, Eds., vol. 10931, International Society for Optics and Photonics. SPIE, 2019, pp. 1 – 9. [Online]. Available: https://doi.org/10.1117/12.2509577

[21] A. Kueter, S. Reible, T. Geibig, D. Nuessler, and N. Pohl, "Thz imaging for recycling of black plastics," *tm - Technisches Messen*, vol. 85, no. 3, pp. 191 – 201, 2018.

[22] A. Geiger, P. Lenz, and R. Urtasun, "Are we ready for autonomous driving? the kitti vision benchmark suite," in *Conference on Computer Vision and Pattern Recognition (CVPR)*, 2012.

[23] E. J. Candès *et al.*, "Compressive sampling," in *Proceedings of the international congress of mathematicians*, vol. 3. Madrid, Spain, 2006, pp. 1433–1452.

[24] R. C. Lau and T. Woodward, "A new approach to apply compressive sensing to lidar sensing," in *Compressive Sensing III*, vol. 9109. International Society for Optics and Photonics, 2014, p. 91090U.

[25] E. Van Den Berg and M. P. Friedlander, "Probing the pareto frontier for basis pursuit solutions," *SIAM Journal on Scientific Computing*, vol. 31, no. 2, pp. 890–912, 2009.

[26] E. Altuntac, "Choice of the parameters in a primal-dual algorithm for bregman iterated variational regularization," *Numerical Algorithms*, vol. 86, no. 2, pp. 729–759, 2021.

[27] F. Ma, G. V. Cavalheiro, and S. Karaman, "Self-supervised sparse-to-dense: Self-supervised depth completion from lidar and monocular camera," in *2019 International Conference on Robotics and Automation (ICRA)*. IEEE, 2019, pp. 3288–3295.
[28] J. Tang, F.-P. Tian, W. Feng, J. Li, and P. Tan, "Learning guided convolutional network for depth completion," *IEEE Transactions on Image Processing*, vol. 30, pp. 1116–1129, 2020.
[29] J. Uhrig, N. Schneider, L. Schneider, U. Franke, T. Brox, and A. Geiger, "Sparsity invariant cnns," in *2017 international conference on 3D Vision (3DV)*. IEEE, 2017, pp. 11–20.
[30] G. Ros, L. Sellart, J. Materzynska, D. Vazquez, and A. M. Lopez, "The synthia dataset: A large collection of synthetic images for semantic segmentation of urban scenes," in *Proceedings of the IEEE conference on computer vision and pattern recognition*, 2016, pp. 3234–3243.